Title

VWI-APP: Vessel wall imaging-dedicated automated processing pipeline for intracranial atherosclerotic plaque quantification.

Journal

Medical Physics, 50(3)

Authors

Zhou, Hanyue
Xiao, Jiayu
Ganesh, Siddarth
et al.

Publication Date

2023-03-01

DOI

10.1002/mp.16074

Peer reviewed

HHS Public Access

Author manuscript

Med Phys. Author manuscript; available in PMC 2024 March 01.

Published in final edited form as:

Med Phys. 2023 March ; 50(3): 1496–1506. doi:10.1002/mp.16074.

VWI-APP: Vessel Wall Imaging-Dedicated Automated Processing Pipeline for Intracranial Atherosclerotic Plaque Quantification

Hanyue Zhou[1,*], **Jiayu Xiao**[2,*], **Siddarth Ganesh**[3], **Alexander Lerner**[2], **Dan Ruan**[1,4,†], **Zhaoyang Fan**[2,3,5,†]

[1]Department of Bioengineering, University of California, Los Angeles, Los Angeles, CA 90095, USA

[2]Department of Radiology, University of Southern California, Los Angeles, CA 90033, USA

[3]Department of Biomedical Engineering, University of Southern California, Los Angeles, CA 90089, USA

[4]Department of Radiation Oncology, University of California, Los Angeles, CA 90095, USA

[5]Department of Radiation Oncology, University of Southern California, Los Angeles, CA 90033, USA

Abstract

Background: Quantitative plaque assessment based on 3D magnetic resonance (MR) vessel wall imaging (VWI) has been shown to provide valuable numerical markers of the burden and risk of intracranial atherosclerotic disease (ICAD). However, plaque quantification is currently time-consuming and observer-dependent due to the demand for heavy manual effort. A VWI-dedicated automated processing pipeline (VWI-APP) is desirable.

Purpose: To develop and evaluate a VWI-APP for end-to-end quantitative analysis of intracranial atherosclerotic plaque.

Methods: We retrospectively enrolled 91 subjects with ICAD (80 for pipeline development, 10 for an end-to-end pipeline evaluation, and 1 for demonstrating longitudinal plaque assessment) who had undergone VWI and MR angiography. In an end-to-end evaluation, diameter stenosis (DS), normalized wall index (NWI), remodeling ratio (RR), plaque-wall contrast ratio (CR), and total plaque volume (TPV) were quantified at each culprit lesion using the developed VWI-APP and a computer-aided manual approach by a neuroradiologist, respectively. The time consumed in each quantification approach was recorded. Two-sided paired t-tests and intraclass correlation coefficient (ICC) were used to determine the difference and agreement in each plaque metric between VWI-APP and manual quantification approaches.

Corresponding authors' information: Zhaoyang Fan, Address: 2250 Alcazar Street, CSC Room 104, Los Angeles, CA 90033, USA, Tel: 3234428186, Zhaoyang.Fan@med.usc.edu, **Dan Ruan,** Address: 200 UCLA Medical Plaza, B265-79, Los Angeles, CA, 90095, USA, Tel: 3109831456, druan@mednet.ucla.edu.

*Hanyue Zhou and Jiayu Xiao contributed equally to this paper.

†Dan Ruan and Zhaoyang Fan contributed equally to this paper.

CONFLICT OF INTEREST

The authors have no conflicts to disclose.

Results: There was no significant difference between VWI-APP and manual quantification in each plaque metric. The ICC was 0.890, 0.813, 0.827, 0.891, and 0.991 for DS, NWI, RR, CR, and TPV, respectively, suggesting good to excellent accuracy of the pipeline method in plaque quantification. Quantitative analysis of each culprit lesion on average took 675.7 s using the manual approach but shortened to 238.3 s with the aid of VWI-APP.

Conclusions: VWI-APP is an accurate and efficient approach to intracranial atherosclerotic plaque quantification. Further clinical assessment of this automated tool is warranted to establish its utility in the risk assessment of ICAD lesions.

Keywords

MRI; vessel wall imaging; intracranial plaque quantification; deep learning; vessel wall segmentation; centerline tracking

1 INTRODUCTION

Stroke is a leading cause of morbidity and mortality worldwide.[1] Intracranial atherosclerotic disease (ICAD) remains a major risk factor for stroke occurrence. 3D high-resolution, dark-blood magnetic resonance (MR) vessel wall imaging (VWI) has become a non-invasive modality for directly assessing this pathological condition.[2] VWI-based morphological plaque metrics, such as normalized wall index (NWI), vessel wall remodeling ratio (RR) and plaque-wall contrast ratio (CR) have been shown as useful quantitative markers of plaque burden and vulnerability.[3–4] Despite the aid of existing image processing and visualization software, these quantitative analyses still involve heavily manual steps, including image reformation for generating vessel cross-sectional views, vessel lumen and wall contouring, and region-of-interest signal measurement. Therefore, plaque quantification on VWI is currently time-consuming and subject to inter- and intra-observer variations. A VWI-dedicated automated processing pipeline (VWI-APP) is indispensable for fully unleashing the potential of this imaging modality in the clinical management of ICAD.

Previous studies on the development of automated plaque analysis methods focused on relatively large arterial vessels. For example, a conventional model fitting method was developed to quantify the wall thickness of the common carotid artery and descending aorta from axial MR images.[5] The lumen centerline and radii for the target carotid artery are estimated by Hough Transform, and the boundaries of the lumen and outer wall are fitted by a 3D cylindrical B-spline surface. The algorithm is applicable for straight vessel segments and can have a misfit when the shape assumptions are violated in torturous intracranial arteries. Another group used the Dijkstra's algorithm to find the internal and external carotid centerlines with medialness and intensity-based cost functions and segmented the lumen using geodesic active contours based on multispectral MR.[6] However, the active contour-based segmentation approach requires iterative computation with a long computational time. A more recent work focused on multi-contrast and multi-time point image registration to facilitate intracranial atherosclerotic plaque analysis, but still relied on manual delineation and physician's observation.[7]

Deep learning has increasingly been utilized to achieve automated lesion detection, fast centerline tracking, or vessel wall segmentation on VWI.[8–9] Excellent accuracy and time efficiency have been demonstrated in individual tasks. Integrating state-of-the-art neural networks into a plaque analysis pipeline may help substantially improve the overall performance.

In this work, we developed and assessed an integrated VWI-APP to maximally automate the entire intracranial atherosclerotic plaque analysis workflow and provide quantitative morphological metrics.

2 MATERIALS AND METHODS

2.1 Subjects

Under an IRB approval, 91 patients diagnosed with ICAD were retrospectively identified from clinical PACS with additional inclusion criteria: 1) patients received both 3D T1-weighted MR VWI and 3D time-of-flight (TOF) MR angiography (MRA) in the same imaging session, 2) both MR VWI and MRA images were of diagnostic quality. All images were acquired using a 3-Tesla whole-body system (MAGNETOM Prisma; Siemens Healthcare, Erlangen, Germany) and a 64-channel head-neck coil. MR VWI data were collected using a whole-brain VWI protocol with an isotropic spatial resolution of 0.55 mm,[10,11] and MRA data were collected with an isotropic spatial resolution of 0.6 mm after interpolation. Detailed imaging parameters are summarized in Supplementary Table S-1. The 91 patients were split into 80 for the development of centerline tracking (5 for training, 10 for testing) and vessel segmentation (74 for training, 3 for validation, and 3 for testing) modules, 10 for an end-to-end evaluation, and 1 for demonstrating the use of VWI-APP in longitudinal plaque assessment.

2.2 Pipeline Modules

The pipeline consists of five modules (Figure 1): 1) “image registration” between VWI and MRA, 2) “centerline tracking” on MRA, 3) “vessel straightening and slicing” along the extracted centerline on VWI, 4) “vessel wall and lumen segmentation” on cross-sectional VWI slices, and 5) “plaque quantification”. The pipeline toolbox was implemented on 3D Slicer (version 4.11.0), a free, open-source software package for imaging research.[12] Our technological innovations are mainly focused on modules 2) and 4), where centerline tracking utilizes the Dijkstra’s algorithm with an optimized cost function on MRA, and vessel lumen and wall segmentation incorporates the inclusion relationship between inner and outer vessel boundaries and provides feasible vessel morphology to support subsequent feature quantification.

2.2.1 Image registration—Image registration is performed to align bright-blood MRA with dark-blood VWI in preparation for accurate centerline tracking on MRA. Specifically, rigid registration with no initialization transform, available from 3D Slicer, is employed to align the two image sets. Mutual information is used to quantify similarity and is maximized during the registration process.

2.2.2 Centerline tracking—Centerline tracking is formulated as a dynamic programming problem to identify the most viable path between the given start and end points, and the Dijkstra's algorithm was to solve it.[13] Specifically, the nodes are the user-input start and end points of a selected vessel segment of interest. The Dijkstra's algorithm is performed on the registered MRA, exploiting its high signal contrast between the artery and surrounding tissues. To improve the robustness in various MRA cases with a fixed set of hyperparameters, serving as the default selection in the software, MRA is further Z-score normalized, denoted as mra_{norm}.

We propose a cost function for the Dijkstra's algorithm based on MRA intensities as shown in Eq. (1):

$$\mathscr{L}_{Dijkstra} = \begin{cases} c, mra_{norm} < thr_l; \\ exp^{-1}(a \cdot D), mra_{norm} > thr_h; \\ 1, else\,. \end{cases} \quad (1)$$

The central logic is to establish two barriers for vessel centerline tracking: a) a foreground vs. background barrier established by image signal intensity threshold thr_l to assign a high cost c to the background; and b) a centerline vs. edge barrier inside a vessel by the Euclidean distance transform D with an inverse exponential function. The coefficient a is an empirically chosen hyperparameter that controls the gap between center points and edge points. thr_h is another empirically chosen threshold hyperparameter which is slightly higher than the background threshold thr_l to ensure a good separation between two adjacent vessel segments during distance transform.

A coarse-to-fine scheme is adopted. It first performs centerline tracking on a down-sampled volume by 0.2 times, followed by cropping the whole volume into a cube encompassing the detected centerline and another round of centerline search on the full-resolution cropped cube. This scheme avoids long computational time on the entire volume search, and also enhances the tracking robustness to highly torturous vessels, where a direct cropping would otherwise miss some portions of a vessel structure.

The default hyper-parameters were set at $c = 10^{-3}$, $a = 5$, $\text{thr}_l = 2$, and $\text{thr}_h = 4$, based on the training performance of 5 random samples.

2.2.3 Vessel straightening and slicing—Vessel straightening and slicing are performed along the derived centerline with a 3D Slicer extension.[14] This module identifies the normal directions, aligns curve centers, and reconstructs contiguous cross-sectional slices with 128×128 in image size, 0.55 mm in thickness, and 0.1 mm in-plane resolution.

2.2.4 Vessel wall and lumen segmentation—Vessel wall and lumen segmentation is performed using our recently developed deep learning method that particularly models the inclusion relationship between the segmented classes with a multiple level set approach.[15] The network structure adopts a UNet structure with a ResNet backbone,[16,17] and has a single output channel with sigmoid activation, as illustrated in Figure 2, for a level-set inference.

The inclusion morphology between the inner and outer boundaries of the vessel wall is incorporated with a level-set function $\varphi(x)$: $R^2 \rightarrow R$ under different heights η_1 and η_2, as illustrated in Figure 2. Each predicted class is inferred from indicator composition:

$$\begin{cases} y'_{lumen} = S(\eta_1 - y) \\ y'_{vesselwall} = S(\eta_2 - y) \cdot S(y - \eta_1), \\ y'_{background} = S(y - \eta_2) \end{cases} \quad (2)$$

where S is a relaxed indicator function.

The segmentation network is trained to minimize the objective:

$$L = L^{fidelity} + \lambda L^{smooth} + \gamma L^{Length}, \quad (3)$$

where L^{Fidelity} is the sum of soft Dice coefficient loss for each class, L^{Smooth} encourages vessel wall encounter when transiting between the background and lumen, and L^{Length} penalizes roughness of the vessel wall boundaries.[18,19]

The 2.5D UNet takes three consecutive slices as the input and output the class prediction for the middle slice. It has 32 base number of channels. For each convolution block, element-wise summation is used to incorporate information from the previous convolution layer to the last convolution layer. The network was trained with a learning rate of 10^{-4} over 50 epochs, using Adam optimizer and a batch size of 32. The hyperparameters in the cost function were $\lambda = 0.5$ and $\gamma = 0.5$. The pipeline stores the structure and the weights of the trained network for inference. Note that the user is allowed to modify the vessel and lumen contours in 3D Slicer when appropriate.

2.2.5 Plaque quantification—Following the processing steps above, a vessel segment selected by the user will undergo plaque quantification. Our algorithm first proposes both the most stenotic slice and a reference slice across the vessel segment based on the lumen area. Users are allowed to modify these slice locations as appropriate. A group of clinically relevant morphological plaque metrics, i.e., diameter stenosis (DS), NWI, RR, CR, and total plaque volume (TPV) as illustrated in Supplementary Figure S-1, are then automatically derived and output. DS and NWI are the measures of plaque burden.[20] RR reflects the extent of vessel narrowing or expansion associated with plaque growth.[21,22] High CR value may be associated with intraplaque hemorrhage that indicates plaque vulnerability.[5] TPV is an absolute measure of plaque burden. Given the area of individual slices readily available after vessel segmentation, the calculations of NWI, RR and TPV are straightforward. For DS quantification, the lumen diameter is calculated by approximating the vessel and lumen contours as circles.[23] CR is calculated as the mean of a high signal intensity cluster in the most stenotic slice divided by that of the reference slice. The high cluster is obtained by thresholding, where intra-class variance is minimized, known as the Otsu's thresholding approach.[24] A connected component analysis (CCA) is further applied to retain a single cluster with the highest intensities in a slice. This process is illustrated in Supplementary Figure S-2.

2.3 Pipeline Evaluation

We first evaluated the performance of the two key VWI-APP modules, i.e., centerline tracking and deep learning-based vessel segmentation. The end-to-end performance of the VWI-APP was then evaluated through a comparison with a computer-aided manual approach. Finally, the pipeline was applied to a patient with two VWI examinations 5 months apart to demonstrate its utility in monitoring plaque morphological changes.

2.3.1 Evaluation of the centerline tracking module—This module was evaluated on 10 randomly selected patients. In each case, left and right intracranial internal carotid artery (ICA) and middle cerebral artery (MCA) (M1 and M2 segment) were included, with approximately 10 cm in total length for each side.

The centerline tracking algorithm was evaluated using the averaged l_2 distance and the maximum l_2 distance between the VWI-APP centerline and the centerline manually traced by a radiologist (8 years of experience in vessel wall image analysis). The point-wise correspondence was established by finding the nearest point of the VWI-APP centerline to each point in the manual centerline which typically consists of 10 to 15 points. The evaluation was performed on long vessel segments covering both the normal and stenotic segments.

2.3.2 Evaluation of the segmentation module—In each of 80 patients, the following arterial segments including the one that involved the identified plaque were used for network training (74), validation (3), and testing (3): the intracranial ICA, MCA, the intracranial vertebral artery, and the basilar artery. Each segment contributed 30 consecutive cross-sectional slices. The “ground truth” lumen and vessel wall were labeled by the same radiologist. The evaluation of the segmentation network adopted Dice similarity coefficient (DSC), 95 percentile Hausdorff distance (HD 95), and mean surface distance (MSD).

2.3.3 End-to-end evaluation—The end-to-end evaluation of VWI-APP was performed in 10 additional patients with symptomatic ICAD. The analysis was focused on the vessel segments where the culprit plaque was located, including the MCA M1 segment in 6 patients and the intracranial ICA, MCA-M2, intracranial vertebral artery, and basilar artery in 4 patients, respectively. Each analyzed vessel segment was approximately 2 cm long.

A comparison in culprit lesion quantitative analysis was made between the VWI-APP approach and the manual approach performed by the same radiologist with a two-week time interval. During manual quantification, the centerline was manually traced followed by computer-aided vessel straightening and cross-sectional view generation in 3D Slicer (version 4.11.0).[12] The cross-sectional images were then exported to Horos (version 3.3.6) for manual measurement of area and signal intensity in hand-drawn regions of interest. With the VWI-APP approach, the radiologist was allowed to manually adjust segmentation contours and/or the locations of the most stenotic and reference slices. With both approaches, DS, NWI, RR, CR, and TPV were calculated. The time consumed by using each of the two approaches was recorded.

2.3.4 Longitudinal plaque assessment—

To demonstrate the usefulness of our toolbox, we selected a patient with acute left corona radiata infarction attributed to a culprit plaque in the left MCA M1 segment to analyze the changes in plaque features over a 5-month time interval. Care was taken to ensure consistency of measurement locations between the two time points. The patient recovered well under medical treatment and did not have any recurrence during 18 months of follow-up.

2.4 Statistical Test

Two-sided paired t-tests with the significance level defined at $\alpha < 0.05$ were used to compare each quantitative metric as well as the time consumed between the manual and VWI-APP approaches. Intraclass correlation coefficient (ICC) with the single-rater two-way mixed model between the two approaches and the corresponding 95% confidence intervals (CI_95) were reported.[25] The mean absolute error (MAE) of DS, NWI, RR, CR, and TPV metrics were determined.

3 RESULTS

3.1 Centerline Tracking

The average and maximum l_2 distance between the VWI-APP detected and manually traced centerlines for each of the 10 patients are shown in Table 1. Averagely, the developed algorithm achieved a deviation of 0.679-mm from the manual ground-truth in generating the centerline. The stenotic locations more commonly rendered challenges than normal counterparts due to the smaller lumen diameter and the resultant reduced MRA signal intensity. Illustrated in Figure 3 (a) are three test patients representing good, moderate, and poor tracking quality, respectively. Patient 2 and Patient 10 had larger discrepancies between the two approaches, presumably due to substantially weak vessel signals in MRA, as illustrated in Figure 3 (b). In such scenarios, manual adjustment at a few control points on the VWI-APP centerline can be performed using the software user interface.

3.2 Vessel Wall and Lumen Segmentation

The performance of the segmentation module is illustrated in Figure 4. The predicted segmentation well resembled the ground truth, and better preserved the geometric integrity. The DSC was 0.925 ± 0.048 for the lumen and 0.786 ± 0.084 for the vessel wall, respectively. The 95% HD was 0.286 ± 0.436 mm and 0.345 ± 0.419 mm, and the MSD was 0.083 ± 0.037 mm and 0.103 ± 0.032 mm, respectively.

3.3 End-to-end Evaluation

Quantitative plaque metrics are reported in Table 2. There was no significant difference between VWI-APP quantification and manual quantification (DS: $p = 0.543$, NWI: $p = 0.058$, RR: $p = 0.161$, CR: $p = 0.539$, TPV: $p = 0.506$). The ICCs were 0.890, 0.813, 0.827, 0.891, and 0.991 for DS, NWI, RR, CR, and TPV measures, respectively, indicating good to excellent agreement with the manual ground-truth.[25] When performing quantification of DS, NWI, RR, CR, and TPV, the average processing time for the 10 test subjects was significantly reduced from 675.7 s ± 204.0 s with manual quantification to 238.3 s ± 77.8 s

with VWI-APP quantification. In 3 out of 10 cases, manual adjustment was needed for the centerlines and/or vessel contours.

3.4 Longitudinal Plaque Assessment

Figure 5 illustrates the quantification of two longitudinal VWI scans from a patient. The quantitative measures were 57.91%, 0.773, 0.868, 1.709, and 125.58 mm^3 for the first scan, and 24.60%, 0.682, 0.908, 1.225, and 105.44 mm^3 for the second scan, for DS, NWI, RR, CR, and TPV, respectively. All the analyzed metrics clearly demonstrated a lesion-level improvement that was presumably associated with effective medical treatment.

4 DISCUSSION

In this work, we introduced an integrated VWI-dedicated image processing pipeline for automated quantitative analysis of intracranial atherosclerotic plaque. VWI-APP provides superior performance in quantification accuracy and efficiency with minimal user interaction. This tool would facilitate clinical workflow and further promote clinical adoption of MR VWI in the management of ICAD.

Our technical innovations lie in two of the five modules, specifically, the centerline tracking module and the vessel lumen and wall segmentation module. The centerline tracking module utilized the Dijkstra's algorithm to find the minimum cost path between the given start and end points of a vessel segment,[26] with customized cost functions. This method performed well in practice and can be preferred for its simplicity and interpretability over alternatives such as the deep learning-based methods for predicting direction and radius of an artery.[27] The default hyperparameter selection was found robust to various MRA volume cases. $thr_l = 2$ and $thr_h = 4$ were more sensitive than the other two hyperparameters to image signal intensity and can be slightly tuned within ±2 to different cases. Given that typical diameter is approximately 5 mm for ICA,[28] 1.9 to 3.5 mm for MCA M1 segment,[29] and 1.1 to 2.1 mm for MCA M2 segment,[30] the average centerline distance discrepancy was lower than the vessel radius. The normal segment also had a mean distance smaller than the voxel size of isotropic 0.55 mm. The manual input of the start and end points in the centerline tracking module can be further automated by extracting the whole vessel tree, applying vessel wall segmentation based on VWI to the suspicious stenosis segments determined by MRA analysis, and performing quantitative analysis of each segment. A related work is a deep neural network integrated with vessel tree and centerline extraction and bifurcation detection using 3D MRA volumes.[31]

In the vessel lumen and wall segmentation module, we adopted our recently proposed segmentation method based on deep learning to capture and incorporate the inclusion relationship between classes.[15] Typical lumen and vessel wall segmentation methods either fit active contours to the inner and outer wall boundary based on image intensities and gradients[32–33] or infer the pixel-wise class membership for the lumen and the vessel wall with multiple output channels with deep networks.[34,35] None of the existing methods accounts for the inclusion relationship between the inner and outer boundaries of the vessel wall and can result in clinically infeasible segmentation solutions such as isolated class pixels or lumen outside of the vessel wall. In contrast, our proposed method with the

level-set inference logic can maintain good geometric integrity of the contours as well as segmentation accuracy, to support subsequent clinical quantification.

The time reduction and repeatability using the VWI-APP are compelling features. Our results showed that the manual approach for analyzing a single culprit lesion typically cost over 10 min. This time would be much longer for less experienced readers. In contrast, our automated approach achieved nearly 3-fold improvement. Besides, compared to human analyses which were reported to have moderate to excellent intra- and interobserver reliability with intraclass correlation coefficient varying from 0.57 to 0.99,[36,37,38] VWI-APP offers intrinsic repeatability as an automated computational platform. Given that ICAD is often implicated in multiple arterial segments, whole-brain plaque quantification may become clinically necessary and feasible with this time-efficient analysis pipeline. We are actively incorporating new functional modules in the software, such as image quality checkpoints, multi-contrast and multi-time-point registration and visualization, and curved multi-planar reconstruction. Large-scale multi-institutional validations are warranted to establish the utility of this software tool. As a clinical-service oriented development, we are also actively investigating approaches to improve friendliness.

We demonstrated our initial experience in using VWI-APP to longitudinally track the plaque morphological changes during medical therapy. All interrogated plaque metrics based on VWI-APP indicated appreciable treatment effects. This automated analysis is in principle more reproducible than its manual counterpart and facilitate more objective and confident clinical decision. It is noteworthy that the utility of VWI-APP is not restricted to ICAD but possesses broad applicability for many cerebrovascular diseases that involve vessel wall pathological changes and may benefit from VWI.

Our work has the following limitations in its current form. First, the current pipeline was developed and assessed on intracranial vessels only. Extension to include the extracranial cervical arteries may be clinically desirable. We expect the centerline tracking algorithm to be readily adapted to this use with cervical VWI having larger vessel caliber and higher vessel wall contrast. Nevertheless, further parameter tuning may be necessary, and validation is needed. Second, the automated pipeline was evaluated against manual depiction by a single expert, which is subject to bias. In the future, multi-observer labeling and a consensus protocol may be used to improve the quality of evaluation. Last but not least, the current pipeline interacts with human observer via manual review and modification. In future work, each module can be extended to automatically flag predictions of lower confidence for further human intervention to improve workflow efficiency.

5 CONCLUSIONS

In this study, we developed an automated pipeline, VWI-APP, for end-to-end intracranial plaque quantification. The pipeline provides accurate centerline tracking and vessel structure segmentation, as well as expert-level clinical plaque quantification, with substantially reduced demand on human labor and analysis time.

Supplementary Material

Refer to Web version on PubMed Central for supplementary material.

ACKNOWLEDGMENTS

This work is supported in part by NIH/NHLBI R01 HL147355.

DATA AVAILABILITY STATEMENT

The data that support the findings of this study are available from the corresponding author upon reasonable request.

REFERENCE

1. Murphy SJX, Werring DJ. Stroke: causes and clinical features. Medicine. 2020;48(9):561–566. doi:10.1016/j.mpmed.2020.06.002 [PubMed: 32837228]
2. Bodle JD, Feldmann E, Swartz RH, Rumboldt Z, Brown T, Turan TN. High-Resolution Magnetic Resonance Imaging: An Emerging Tool for Evaluating Intracranial Arterial Disease. Stroke. 2013;44(1):287–292. doi:10.1161/STROKEAHA.112.664680 [PubMed: 23204050]
3. Song JW, Pavlou A, Burke MP, et al. Imaging endpoints of intracranial atherosclerosis using vessel wall MR imaging: a systematic review. Neuroradiology. 2021;63(6):847–856. doi:10.1007/s00234-020-02575-w [PubMed: 33029735]
4. Chung JW, Cha J, Lee MJ, et al. Intensive Statin Treatment in Acute Ischaemic Stroke Patients with Intracranial Atherosclerosis: a High-Resolution Magnetic Resonance Imaging study (STAMINA-MRI Study). J Neurol Neurosurg Psychiatry. 2020;91(2):204–211. doi:10.1136/jnnp-2019-320893 [PubMed: 31371644]
5. Gao S, van ‘t Klooster R, Brandts A, et al. Quantification of common carotid artery and descending aorta vessel wall thickness from MR vessel wall imaging using a fully automated processing pipeline: Quantification of CCA and DAO. J Magn Reson Imaging. 2017;45(1):215–228. doi:10.1002/jmri.25332 [PubMed: 27251901]
6. Tang H, van Walsum T, van Onkelen RS, et al. Semiautomatic carotid lumen segmentation for quantification of lumen geometry in multispectral MRI. Medical Image Analysis. 2012;16(6):1202–1215. doi:10.1016/j.media.2012.05.014 [PubMed: 22841778]
7. Guo Y, Canton G, Chen L, et al. Multi-Planar, Multi-Contrast and Multi-Time Point Analysis Tool (MOCHA) for Intracranial Vessel Wall Characterization. Magnetic Resonance Imaging. Published online January 31, 2022:jmri.28087. doi:10.1002/jmri.28087
8. Chen L, Canton G, Liu W, et al. Fully automated and robust analysis technique for popliteal artery vessel wall evaluation (FRAPPE) using neural network models from standardized knee MRI. Magn Reson Med. 2020;84(4):2147–2160. doi:10.1002/mrm.28237 [PubMed: 32162395]
9. Shi F, Yang Q, Guo X, et al. Intracranial Vessel Wall Segmentation Using Convolutional Neural Networks. IEEE Trans Biomed Eng. 2019;66(10):2840–2847. doi:10.1109/TBME.2019.2896972 [PubMed: 30716027]
10. Yang Q, Deng Z, Bi X, et al. Whole-brain vessel wall MRI: A parameter tune-up solution to improve the scan efficiency of three-dimensional variable flip-angle turbo spin-echo: Expediting 3D TSE-Based Whole-Brain Vessel Wall Imaging. J Magn Reson Imaging. 2017;46(3):751–757. doi:10.1002/jmri.25611 [PubMed: 28106936]
11. Fan Z, Yang Q, Deng Z, et al. Whole-brain intracranial vessel wall imaging at 3 Tesla using cerebrospinal fluid-attenuated T1-weighted 3D turbo spin echo: Whole-Brain Intracranial Vessel Wall Imaging at 3 T. Magn Reson Med. 2017;77(3):1142–1150. doi:10.1002/mrm.26201 [PubMed: 26923198]

12. Kikinis R, Pieper SD, Vosburgh KG. 3D Slicer: A Platform for Subject-Specific Image Analysis, Visualization, and Clinical Support. In: Jolesz FA, ed. Intraoperative Imaging and Image-Guided Therapy. Springer New York; 2014:277–289. doi:10.1007/978-1-4614-7657-3_19
13. Dijkstra EW. A note on two problems in connexion with graphs. Numer Math. 1959;1(1):269–271. doi:10.1007/BF01386390
14. SlicerSandbox: Curved Planar Reformat. https://github.com/PerkLab/SlicerSandbox/blob/master/CurvedPlanarReformat/CurvedPlanarReformat.py
15. Zhou H, Xiao J, Li D, Fan Z, Ruan D. Intracranial Vessel Wall Segmentation with Deep Learning using a Novel Tiered Loss Function Incorporating Class Inclusion. Medical Physics. Published online July 11, 2022:mp.15860. doi:10.1002/mp.15860
16. Ronneberger O, Fischer P, Brox T. U-Net: Convolutional Networks for Biomedical Image Segmentation. Published online 2015. doi:10.48550/ARXIV.1505.04597
17. Niethammer M, Kwitt R, Vialard FX. Metric Learning for Image Registration. In: 2019 IEEE/CVF Conference on Computer Vision and Pattern Recognition (CVPR). IEEE; 2019:8455–8464. doi:10.1109/CVPR.2019.00866
18. Vogel CR, Oman ME. Iterative Methods for Total Variation Denoising. SIAM J Sci Comput. 1996;17(1):227–238. doi:10.1137/0917016
19. Chen X, Williams BM, Vallabhaneni SR, Czanner G, Williams R, Zheng Y. Learning Active Contour Models for Medical Image Segmentation. In: 2019 IEEE/CVF Conference on Computer Vision and Pattern Recognition (CVPR). IEEE; 2019:11624–11632. doi:10.1109/CVPR.2019.01190
20. Xiao J, Padrick MM, Jiang T, et al. Acute ischemic stroke versus transient ischemic attack: Differential plaque morphological features in symptomatic intracranial atherosclerotic lesions. Atherosclerosis. 2021;319:72–78. doi:10.1016/j.atherosclerosis.2021.01.002 [PubMed: 33486353]
21. Qiao Y, Anwar Z, Intrapiromkul J, et al. Patterns and Implications of Intracranial Arterial Remodeling in Stroke Patients. Stroke. 2016;47(2):434–440. doi:10.1161/STROKEAHA.115.009955 [PubMed: 26742795]
22. Mintz GS, Kent KM, Pichard AD, Satler LF, Popma JJ, Leon MB. Contribution of Inadequate Arterial Remodeling to the Development of Focal Coronary Artery Stenoses: An Intravascular Ultrasound Study. Circulation. 1997;95(7):1791–1798. doi:10.1161/01.CIR.95.7.1791 [PubMed: 9107165]
23. Ouhlous M, Lethimonnier F, Dippel DWJ, et al. Evaluation of a dedicated dual phased-array surface coil using a black-blood FSE sequence for high resolution MRI of the carotid vessel wall. J Magn Reson Imaging. 2002;15(3):344–351. doi:10.1002/jmri.10067 [PubMed: 11891981]
24. Otsu N A Threshold Selection Method from Gray-Level Histograms. IEEE Trans Syst, Man, Cybern. 1979;9(1):62–66. doi:10.1109/TSMC.1979.4310076
25. Koo TK, Li MY. A Guideline of Selecting and Reporting Intraclass Correlation Coefficients for Reliability Research. Journal of Chiropractic Medicine. 2016;15(2):155–163. doi:10.1016/j.jcm.2016.02.012 [PubMed: 27330520]
26. Diedrich KT, Roberts JA, Schmidt RH, Parker DL. Comparing Performance of Centerline Algorithms for Quantitative Assessment of Brain Vascular Anatomy. Anat Rec. 2012;295(12):2179–2190. doi:10.1002/ar.22603
27. Wolterink JM, van Hamersvelt RW, Viergever MA, Leiner T, Išgum I. Coronary artery centerline extraction in cardiac CT angiography using a CNN-based orientation classifier. Medical Image Analysis. 2019;51:46–60. doi:10.1016/j.media.2018.10.005 [PubMed: 30388501]
28. Krejza J, Arkuszewski M, Kasner SE, et al. Carotid Artery Diameter in Men and Women and the Relation to Body and Neck Size. Stroke. 2006;37(4):1103–1105. doi:10.1161/01.STR.0000206440.48756.f7 [PubMed: 16497983]
29. Valvita R, Sadi B. Variations of shape, length, branching, and end trunks of M1 segment of middle cerebral artery. J Neurol Neurol Sci Disord. 2019;5(1):052–056. doi:10.17352/jnnsd.000034
30. Mut F, Wright S, Ascoli GA, Cebral JR. Morphometric, geographic, and territorial characterization of brain arterial trees: CHARACTERIZATION OF BRAIN ARTERIAL TREES. Int J Numer Meth Biomed Engng. 2014;30(7):755–766. doi:10.1002/cnm.2627

31. Tetteh G, Efremov V, Forkert ND, et al. DeepVesselNet: Vessel Segmentation, Centerline Prediction, and Bifurcation Detection in 3-D Angiographic Volumes. Front Neurosci. 2020;14:592352. doi:10.3389/fnins.2020.592352 [PubMed: 33363452]

32. Adame IM, van der Geest RJ, Wasserman BA, Mohamed MA, Reiber JHC, Lelieveldt BPF. Automatic segmentation and plaque characterization in atherosclerotic carotid artery MR images. Magn Reson Mater Phy. 2004;16(5):227–234. doi:10.1007/s10334-003-0030-8

33. Wang Y, Seguro F, Kao E, et al. Segmentation of lumen and outer wall of abdominal aortic aneurysms from 3D black-blood MRI with a registration based geodesic active contour model. Medical Image Analysis. 2017;40:1–10. doi:10.1016/j.media.2017.05.005 [PubMed: 28549310]

34. Chen L, Zhao H, Jiang H, et al. Domain adaptive and fully automated carotid artery atherosclerotic lesion detection using an artificial intelligence approach (LATTE) on 3D MRI. Magnetic Resonance in Med. 2021;86(3):1662–1673. doi:10.1002/mrm.28794

35. Wu J, Xin J, Yang X, et al. Deep morphology aided diagnosis network for segmentation of carotid artery vessel wall and diagnosis of carotid atherosclerosis on black-blood vessel wall MRI. Med Phys. 2019;46(12):5544–5561. doi:10.1002/mp.13739 [PubMed: 31356693]

36. Wu F, Ma Q, Song H, et al. Differential Features of Culprit Intracranial Atherosclerotic Lesions: A Whole-Brain Vessel Wall Imaging Study in Patients With Acute Ischemic Stroke. J Am Heart Assoc. 2018;7(15). doi:10.1161/JAHA.118.009705

37. Qiao Y, Steinman DA, Qin Q, et al. Intracranial arterial wall imaging using three-dimensional high isotropic resolution black blood MRI at 3.0 Tesla. J Magn Reson Imaging. 2011;34(1):22–30. doi:10.1002/jmri.22592 [PubMed: 21698704]

38. Shi Z, Zhao M, Li J, et al. Association of Hypertension With Both Occurrence and Outcome of Symptomatic Patients With Mild Intracranial Atherosclerotic Stenosis: A Prospective Higher Resolution MAGNETIC RESONANCE IMAGING Study. J Magn Reson Imaging. Published online March 10, 2021:jmri.27516. doi:10.1002/jmri.27516

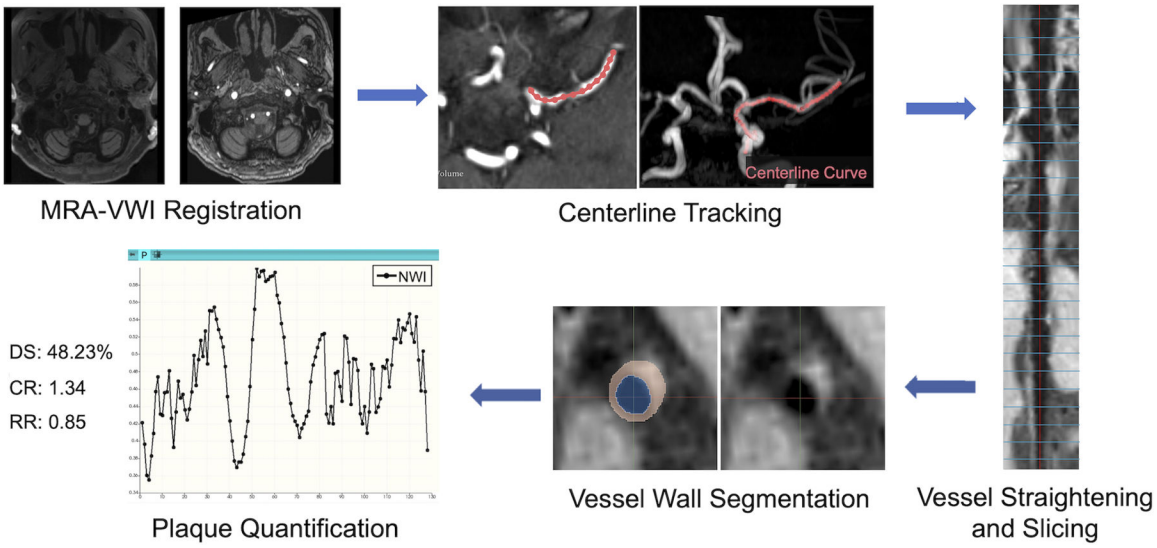

Figure 1.

The diagram of VWI-APP workflow and key techniques. Following image registration between MRA and VWI, the centerline of a selected vessel segment is automatically tracked on MRA. On the co-registered VWI, the segment is then straightened along the derived centerline and sliced into cross-sectional sections that later undergo vessel wall and lumen segmentation and plaque quantification. DS = diameter stenosis, NWI = normalized wall index, CR = plaque-wall contrast ratio, RR = remodeling ratio.

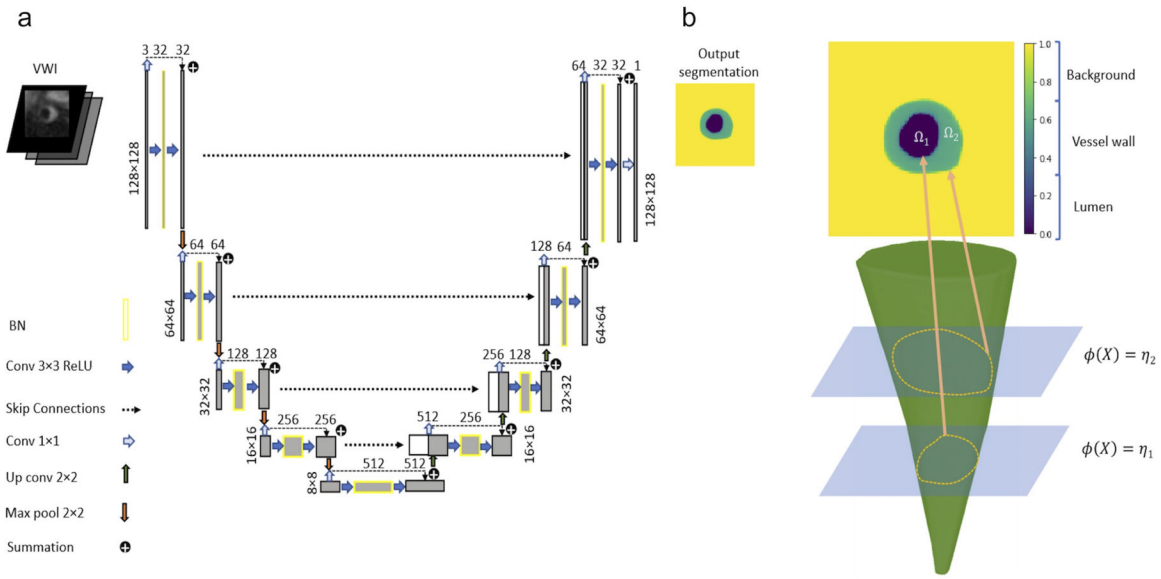

Figure 2.

The segmentation network uses a level-set logic to establish the inclusion relationship between the inner and outer boundary of the vessel wall. (a) UNet structure with skip connections in each convolution block to pass the features learned in previous layers; and (b) network single-channel output y and the corresponding lumen and vessel delineation.

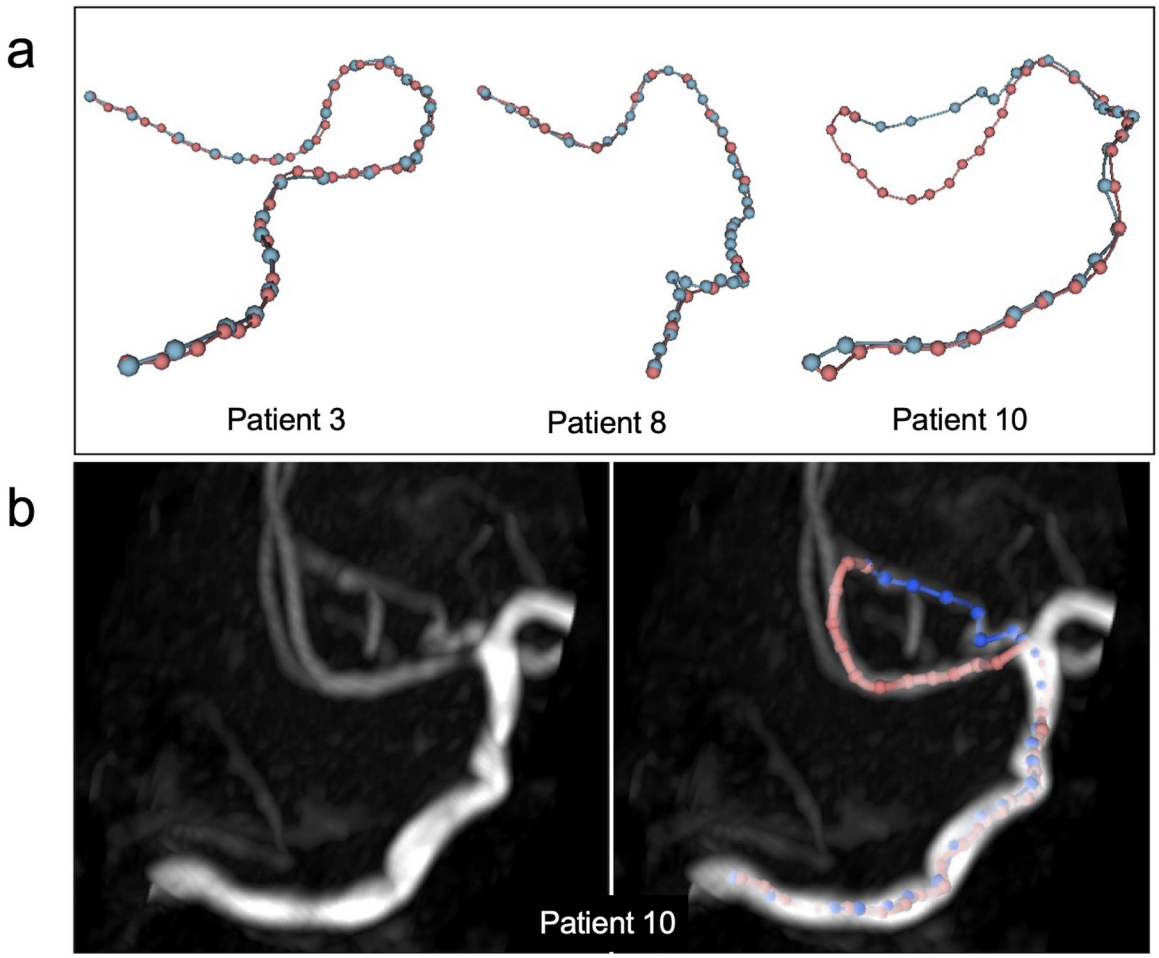

Figure 3.

Qualitative illustration of centerline tracking results: (a) are the results of three representative test cases, where the blue and red lines are the manual and algorithm detected centerlines, respectively; (b) is an illustration of possible centerline tracking error caused by MRA signal loss, where the ground truth is the upper blue line, and the algorithm detected is the lower red line.

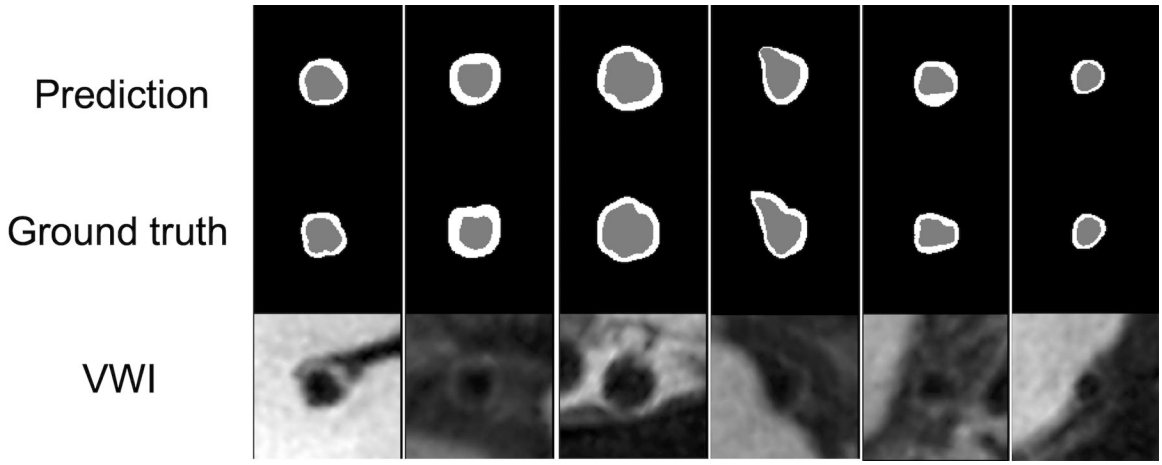

Figure 4.
Qualitative performance of the segmentation module by our proposed tiered segmentation method: each column is an example slice. Gray denotes the lumen, white the vessel wall, and black the background.

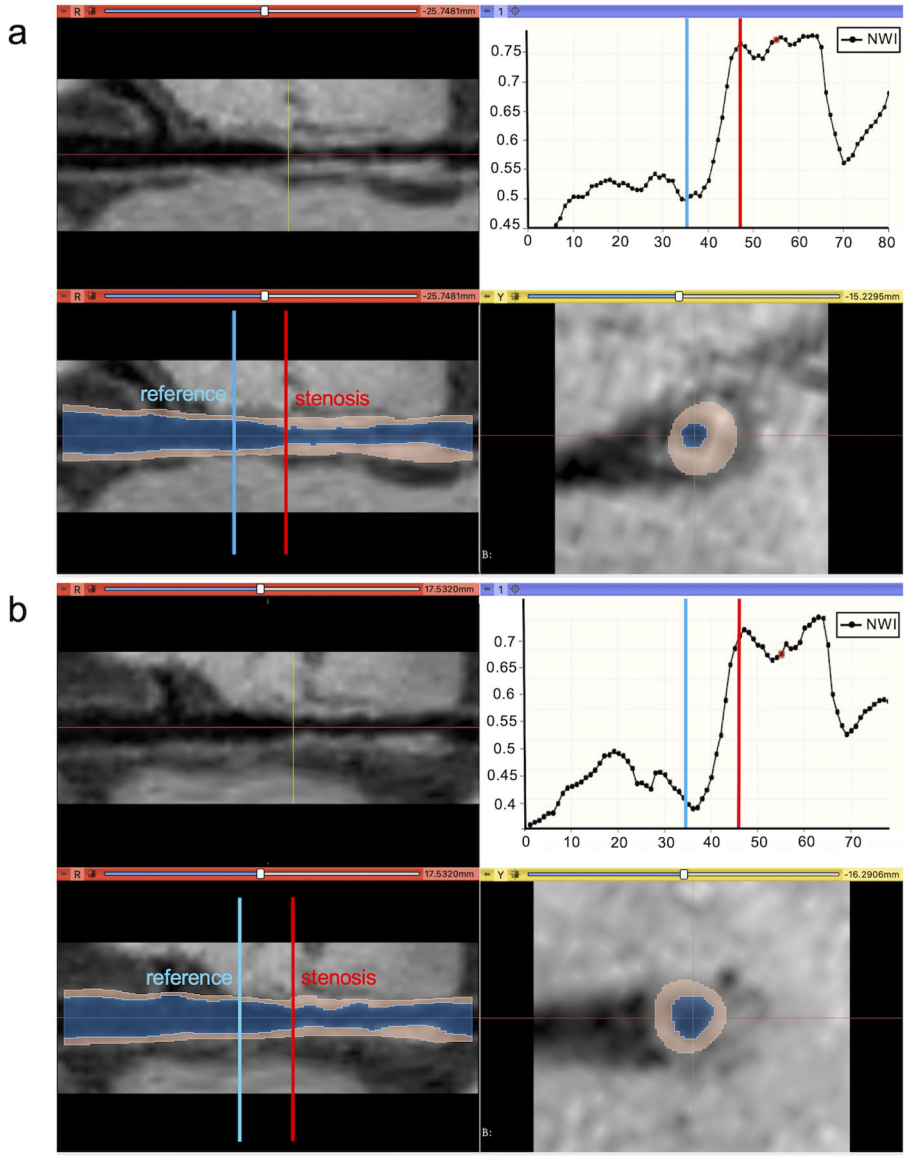

Figure 5.

Demonstration of plaque monitoring of a patient. There was a 5-month interval between baseline VWI (a) and follow-up VWI (b). The straightened vessel is shown in the left panels both before and after segmentation. The bottom right panel shows a cross-sectional slice with segmentation mask. Results of the plaque quantification are displayed in the upper right panel. The stenotic slice (red vertical line) was generated by the pipeline toolbox at the smallest lumen area across the whole segment, and the reference slice (blue vertical line) was manually adjusted. The follow-up VWI was registered to the baseline VWI, and (b) has the same stenosis and reference slice selection as (a).

Table 1.

The average and maximum distances between the VWI-APP detected centerline and the manually traced centerline in 10 test patients.

	Whole vessel (mm)		Stenotic segment (mm)	
Patient	**Average**	**Maximum**	**Average**	**Maximum**
1	0.437	1.281	0.623	1.281
2	2.062	10.400	4.229	10.400
3	0.343	0.640	0.310	0.349
4	0.622	2.310	0.319	0.394
5	0.434	1.196	0.663	1.196
6	0.403	1.393	0.452	0.736
7	0.335	0.643	0.317	0.438
8	0.447	1.622	0.609	1.622
9	0.420	0.764	0.428	0.695
10	1.292	7.296	0.370	0.650
Average	0.679	2.754	0.832	1.776
Standard deviation	0.562	3.332	1.201	3.059

Table 2.

End-to-end evaluation of VWI-APP in 10 patients with symptomatic ICAD.

	DS (%)		NWI		RR		CR		TPV (mm^3)	
Patient	**Manual**	**Pipeline**	**Manual**	**Pipeline**	**Manual**	**Pipeline**	**Manual**	**Pipeline**	**Manual**	**Pipeline**
1	18.65	7.20	0.773	0.679	1.007	1.081	1.879	1.929	91.34	86.44
2	30.63	47.61	0.621	0.708	0.778	0.437	1.496	1.812	100.94	115.72
3	12.28	11.28	0.684	0.640	1.317	1.289	1.337	1.391	48.91	48.19
4	18.83	19.59	0.783	0.633	0.885	0.763	1.937	2.302	110.55	95.34
5	27.41	28.73	0.950	0.820	1.286	1.094	1.749	1.953	100.55	105.83
6	22.94	16.71	0.729	0.693	0.924	0.911	1.929	1.741	32.16	28.63
7	63.35	58.52	0.913	0.895	0.793	0.834	1.809	1.664	84.51	86.89
8	35.01	37.46	0.853	0.807	1.055	1.123	1.297	1.475	109.16	98.74
9	67.21	52.86	0.961	0.929	0.816	0.782	1.235	1.150	449.26	495.60
10	41.55	40.69	0.842	0.841	1.075	1.000	2.978	2.678	183.36	186.95
MAE	6.02 ± 6.10		0.064 ± 0.047		0.099 ± 0.095		0.188 ± 0.105		10.71 ± 12.81	
ICC	0.890		0.813		0.827		0.891		0.991	
CI_95	[0.62, 0.97]		[0.41, 0.95]		[0.45, 0.95]		[0.62, 0.97]		[0.96, 1.00]	

DS = diameter stenosis; NWI = normalized wall index; RR = remodeling ratio; CR = plaque-wall contrast ratio; TPV = total plaque volume; MAE = mean absolute error; ICC = intraclass correlation coefficient; CI = confidence interval.